Cerebral Cortex February 2007;17:400–414
doi:10.1093/cercor/bhj157
Advance Access publication March 17, 2006

Detection of Active and Silent States in Neocortical Neurons from the Field Potential Signal during Slow-Wave Sleep

Mikhail Mukovski[1], Sylvain Chauvette[2], Igor Timofeev[2] and Maxim Volgushev[1,3]

[1]Department of Neurophysiology, Ruhr-University Bochum, Bochum, Germany, [2]Department of Anatomy and Physiology, Laval University, Quebec, Canada and [3]Institute of Higher Nervous Activity and Neurophysiology Russian Academy of Sciences, Moscow, Russia

Oscillations of the local field potentials (LFPs) or electroencephalogram (EEG) at frequencies below 1 Hz are a hallmark of the slow-wave sleep. However, the timing of the underlying cellular events, which is an alternation of active and silent states of thalamocortical network, can be assessed only approximately from the phase of slow waves. Is it possible to detect, using the LFP or EEG, the timing of each episode of cellular activity or silence? With simultaneous recordings of the LFP and intracellular activity of 2–3 neocortical cells, we show that high–gamma-range (20–100 Hz) components in the LFP have significantly higher power when cortical cells are in active states as compared with silent-state periods. Exploiting this difference we have developed a new method, which uses the LFP signal to detect episodes of activity and silence of neocortical neurons. The method allows robust, reliable, and precise detection of timing of each episode of activity and silence of the neocortical network. It works with both surface and depth EEG, and its performance is affected little by the EEG prefiltering during recording. These results open new perspectives for studying differential operation of neural networks during periods of activity and silence, which rapidly alternate on the subsecond scale.

Keywords: active and silent states, EEG and intracellular, oscillations, sleep, state detection

Introduction

Slow fluctuations of the cumulative electrical activity of the brain, local field potentials (LFPs), or electroencephalogram (EEG) are a hallmark of the periods of slow-wave sleep (SWS) (Blake and Gerard 1937). These fluctuations in the LFP or EEG at frequencies ranging from slow (below 1 Hz) to the delta range (1–4 Hz) reflect alternating periods of activity and silence of the thalamocortical networks (Steriade and others 1993a, 2001; Contreras and Steriade 1995; Timofeev and others 2001). Slow rhythmic activity occurs during certain stages of natural sleep, under anesthesia, and even in isolated cortical preparations (Sanchez-Vives and McCormick 2000; Timofeev and others 2000; Mahon and others 2001; Antognini and Carstens 2002). Experimental results demonstrate that the operation of the neural network differs dynamically, depending on the phase of the slow rhythm. Faster rhythms at frequencies >12 Hz are predominantly associated with positive half-waves of the scalp EEG (Mölle and others 2002) or depth-negative EEG waves (Steriade, Amzica, and Contreras 1996; Steriade, Contreras, and others 1996). Further, the amplitude and latency of evoked potentials and neuronal responses depend on the phase of slow oscillation (Timofeev and others 1996; Massimini and others 2003; Sachdev and others 2004; Rosanova and Timofeev 2005). Because the phase of the slow EEG rhythm is related to the alternating episodes of activity and silence of cortical neurons, these results indicate that the operation of a neuronal network depends on whether the neurons are in the active or silent state. However, the relation between the phase of the slow EEG rhythm and the active and silent states in neocortical cells is not regular enough to be formalized into a clear criterion for distinguishing between the states of the neocortical network from the slow EEG waves. The timing of individual episodes of activity and silence, which are readily separable in intracellular recordings by the membrane potential level, escapes precise detection in the slow EEG components, thus leading to contradictory conclusions. For example, according to the phase criterion, field potentials of maximal amplitude were evoked by sensory stimuli applied at the beginning of the active state (Massimini and others 2003), but other studies report suppression of the intracellular responses, either subthreshold or leading to action potentials, during the active states (Petersen and others 2003; Sachdev and others 2004). Drawbacks in the detection of active and silent network states from the phase of slow EEG fluctuations include low temporal precision, failures in cases of low EEG peak amplitude, and high sensitivity of the relative timing between the EEG peaks and onset of the states in cells to the filtering used during the EEG recording. These shortcomings of the state detection restrain progress in understanding differential operation of neural networks during rapidly alternating periods of activity and silence. Using simultaneous LFP and intracellular recordings, we have developed a new method, based on the differential spectral composition of the LFP in the beta/gamma frequency band (20–100 Hz), which allows to separate periods of activity and silence of the neural network during the SWS. We demonstrate the reliability of the method by comparison of the states detected in the LFP and in simultaneously recorded membrane potential of neocortical neurons.

Methods

Experiments were conducted on adult cats, either in chronic experiments during natural sleep and awake states or under ketamine–xylazine anesthesia (10–15 mg/kg ketamine and 2–3 mg/kg xylazine). All experimental procedures used in this study were in accordance with the Canadian guidelines for animal care and were approved by the committee for animal care of Laval University.

Details of the experimental procedures are described elsewhere (Timofeev and others 2001; Crochet and others 2005; Rosanova and Timofeev 2005).

For chronic experiments, preparation was conducted under somnotol (35 mg/kg) anesthesia. The anesthesia was followed by intramuscular (i.m.) injection of buprenorphine (0.03 mg/kg), every 12 h for 24 h, to prevent pain after surgery. Surgery was performed in sterile conditions, and 500 000 units of penicillin i.m. were injected for 3 consecutive days. Under anesthesia, cats were implanted with 1–3 chambers for intracellular recordings and with electrodes for field

potential recording. The chambers and electrodes were placed over various neocortical areas. In addition to the LFP electrodes, pairs of electrodes were placed in ocular cavities and in neck muscles to monitor the states of vigilance by recording the electrooculogram and electromyogram. Several bolts were cemented to the cranium to allow nonpainful fixation of the cat's head in a stereotaxic frame. After a recovery period (7–10 days), cats were adapted for staying in the frame for 1–2 h. Recordings were started after 3–5 days of training, when cats started to sleep in the frame and displayed clear states of waking, SWS and rapid eye movement (REM) sleep. For intracellular recordings, lidocaine was applied focally and a small perforation was made in the dura to allow the insertion of micropipettes. After placing the pipette on the cortical surface, the chamber was filled with warm sterile 4% agar.

In acute experiments, surgery was started after the EEG showed typical signs of general anesthesia and complete analgesia was achieved. Craniotomy was made at coordinates AP −3 to +14, L 3–12, to expose the suprasylvian gyrus. The animals were paralyzed with gallamine triethiodide and artificially ventilated. End-tidal CO_2 was held at 3.5–3.7% and body temperature at 37–38 °C. Additional doses of anesthetics were administrated when the EEG showed changes toward activated patterns. To reduce brain pulsations we made bilateral pneumothorax, hip suspension, and drainage of the cisterna magna. This improved considerably the stability of intracellular recording. Simultaneous recordings of the LFP and intracellular activity of 2–3 neurons were performed. Intracellular and LFP electrodes were positioned in neocortical areas 5, 7, 18, or 21, either at distances 2–4 mm between the electrodes or close (<0.5 mm) to one another. After positioning of the electrodes, the craniotomy was filled with 3.5–4% agar.

At the end of all the experiments the cats were given a lethal dose of pentobarbitone.

LFP's were recorded with coaxial bipolar tungsten electrodes (SNE-100, Rhode Medical Instruments, Summerland, CA). The outer pole of the electrode was positioned on, or 0.1 mm below, the cortical surface and the inner pole was at the depth of 1 mm. Signals were filtered with 2 band-pass filters, one cutting the frequencies below 0.1 kHz and above 10 kHz and the other one reducing the contribution of frequencies around 60 Hz to reduce the mains noise. The LFP signal was amplified with the total gain of 1000.

Intracellular recordings were made with sharp electrodes filled with 2.5 M potassium acetate and 2% neurobiotine and beveled to a resistance of 55–80 MΩ. Intracellular signals were amplified with Neurodata IR-283 amplifiers (Cygnus Technology, Delaware Water Gap, PA). Intracellular and LFP signals were recorded at 20 kHz on a vision data acquisition system (Nicolet, Middleton, WI).

We used for the analysis those recordings in which the LFP signal expressed a clear slow rhythm. As a formal criterion for identification of periods of slow-wave oscillations, we used the ratio between the LFP power below and above 4 Hz. In all recordings selected for analysis, this ratio was higher than 3.5 (see Results, Fig. 1, and related text). During

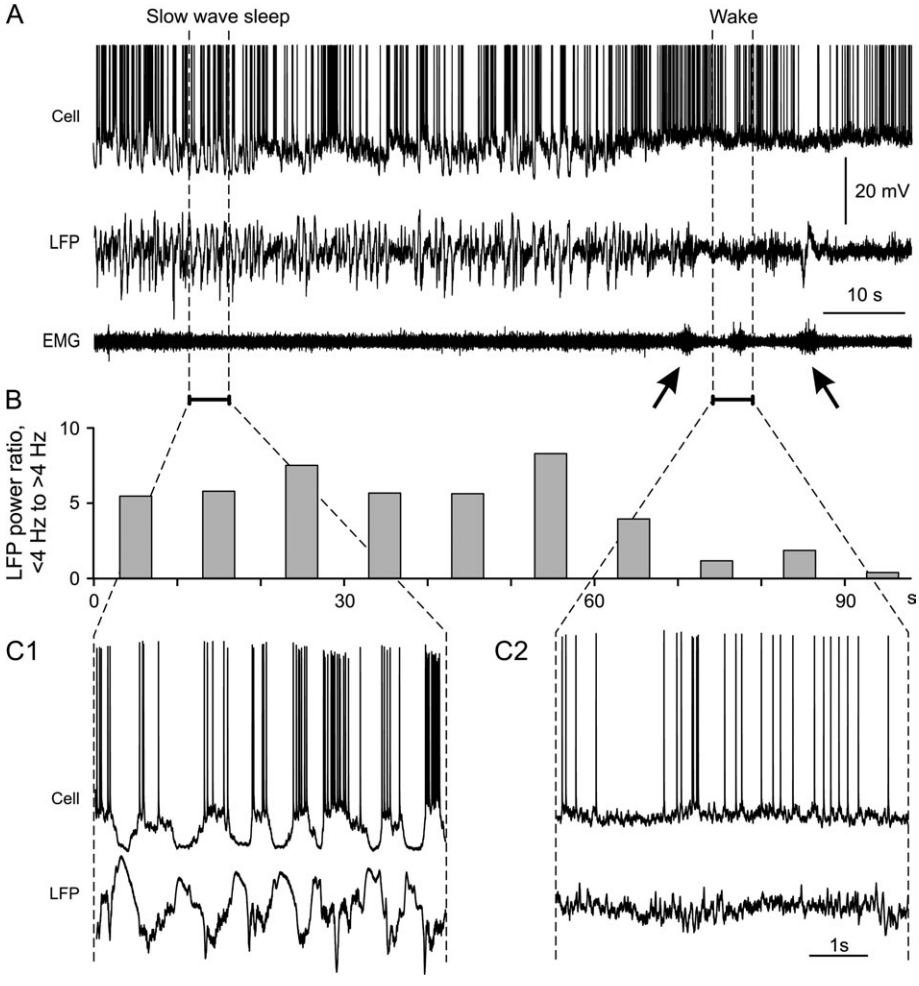

Figure 1. SWS is associated with increased power of the slow components (<4 Hz) in the LFP. (*A*) Simultaneous intracellular, LFP, and EMG recording during natural sleep and wakefulness. SWS at the beginning of the recording turns into awake state from about 70 s, as indicated by activations in the EMG (arrows). Action potentials are truncated. (*B*) Differential spectral composition of the LFP during SWS and wakefulness. For each 10-s period of the LFP recording, power spectra and the ratio of the power at frequencies <4 Hz to the power at frequencies >4 Hz were calculated. Each bar shows the power ratio during the respective period. Same *X*-scale as in (*A*). Note a clear decrease of ratio with awaking of the animal. (*C*1, *C*2) Portions from intracellular activity and LFP recording in (*A*) shown at expanded timescale. Note clear fluctuations of the membrane potential between active and silent states during the SWS but absence of the silent states during the wakefulness.

these periods also the membrane potential distribution in cells showed clear bimodality.

Off-line data processing was done with custom-written programs in MatLab (The MathWorks, Natick, MA) environment.

Results

Slow-Wave Fluctuations in the LFP and in the Membrane Potential of Neocortical Cells

Slow fluctuations of the LFP at frequencies ranging from slow (below 1 Hz) to the delta range (1–4 Hz) are a hallmark of the periods of SWS. Figure 1 illustrates the relation between intracellular activity of a neocortical neuron and the LFP during the SWS and waking. The LFP during the SWS shows characteristic low-frequency, high-amplitude oscillations, which disappear upon transition to the awake state (Fig. 1*A*). Consistent with results of previous studies (Steriade and others 1993a; Contreras and Steriade 1995; Steriade and others 2001; Timofeev and others 2001), the pattern of the membrane potential changes is also fundamentally different during these 2 states of the animal. During the SWS, the membrane potential fluctuates between 2 levels: a depolarized one, associated with cellular activity, and a hyperpolarized one, during which the cell is silent. When the animal is awake, the membrane potential is always around the depolarized level but hyperpolarized states are absent. The difference between the 2 patterns in the LFP and the membrane potential traces, associated with the 2 states of the animal, is especially evident with higher temporal resolution (Fig. 1*C*1,*C*2). To quantify this difference between the SWS and wakefulness, we have calculated the ratio of the LFP power below 4 Hz to the power above 4 Hz. This ratio is high during the SWS (6.0) but becomes low when the animal awakes (1.1). Moreover, the time course of changes of the power ratio corresponds well to the 2 states and the transition from sleep to wakefulness (Fig. 1*B*). Comparison of the slow-wave and REM stages of sleep also revealed a clear difference in the ratio of the LFP power. The contribution of low frequencies was high during the SWS (ratio 11.9) but low during the REM sleep (1.7). Thus, the ratio of LFP power below 4 Hz to the power above 4 Hz allows for a clear detection of the periods of SWS oscillations (see also Olbrich and Achermann 2005).

For further analysis of the slow-wave oscillations, we used data recorded under ketamine–xylazine anesthesia. Under this anesthesia, the LFP shows a typical picture of slow-wave oscillations, but an essential advantage over natural sleep experiments is the possibility of simultaneous intracellular recordings from several, 2–3 in this study, neurons. For the analysis, we selected recordings with the value of the LFP power ratio (<4 Hz/ >4 Hz) higher than 3.5, which is at least 2-fold higher than that observed during the wakefulness or REM sleep. Figure 2 shows an example of simultaneous recording of the LFP and intracellular activity of 2 neocortical neurons. In both neurons, the membrane potential fluctuates between active and silent states (Fig. 2*A*). The active states are associated with depolarized membrane potentials, intensive synaptic activity, and occasional action potentials, whereas during the silent states the neurons are hyperpolarized and generate no action potentials, and synaptic activity in the network is low or absent. Membrane potential levels during active and silent states are separated by 5–25 mV in different cells. The distributions of the membrane potential values are

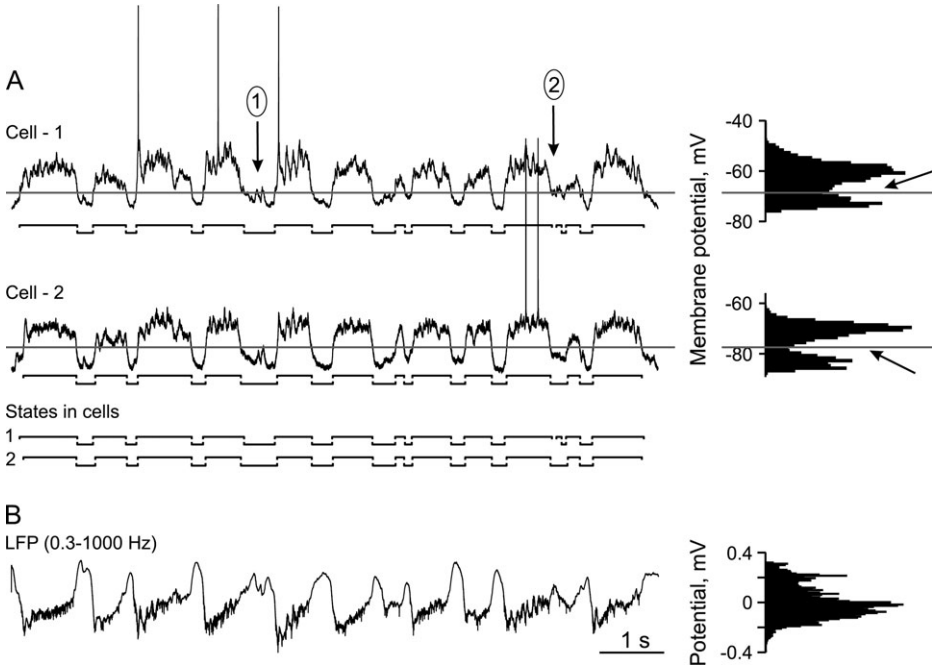

Figure 2. Correlated fluctuations in the membrane potential and LFP. (*A*) Membrane potential traces of 2 simultaneously recorded cells. Histograms on the right-hand side show distributions of membrane potential. Oblique arrows point at clear gaps in the bimodal distributions of the membrane potential of each cell. Levels for the separation of active and silent states were positioned in the bottom of these gaps and are shown with horizontal lines. Active and silent states are indicated with horizontal bars under each membrane potential trace. Arrow (1) points at cases when periods above the level were too short (<40 ms) to be considered as an interruption of a state. Arrow (2) points at cases when periods below the level were too short to be interpreted as a state. The sequences of active and silent states in both cells are also shown in the bottom of panel *A*. Note that occurrence of the states is clearly correlated, but on the fine timescale their synchronization is only loose. (*B*) LFP recorded with a band-pass filter 0.3–1000 Hz simultaneously with the 2 cells shown in (*A*). Histogram on the right-hand side shows distribution of LFP values. Note that although the LFP signal correlates with the occurrence of active and silent states in the cells, its amplitude distribution does not express clear bimodality.

clearly bimodal, allowing for an unambiguous detection and separation of the states (Fig. 2*A*). Because of these different mean levels of the membrane potential, active and silent states are also often referred to as "up" and "down" states, respectively.

Simultaneous intracellular recordings from several cells demonstrate that the active and silent states occur at about the same time in different cells. Comparison of simultaneously recorded membrane potential and LFP traces shows that also the LFP signal looks very different, depending on whether the cells are in the active or in the silent state (Fig. 2*A,B*). However, despite a clear overall correspondence between the LFP and intracellular activity, the level of the LFP signal is not the same at the points of transitions between active and silent states in the cells (see e.g., Figs 3 and 4). Moreover, in contrast to the distribution of the membrane potential values, the distribution of the LFP values does not express clear bimodality. These factors preclude the possibility of precise detection of the timing of each episode of activity or silence in the cells by applying a formal threshold to the LFP signal.

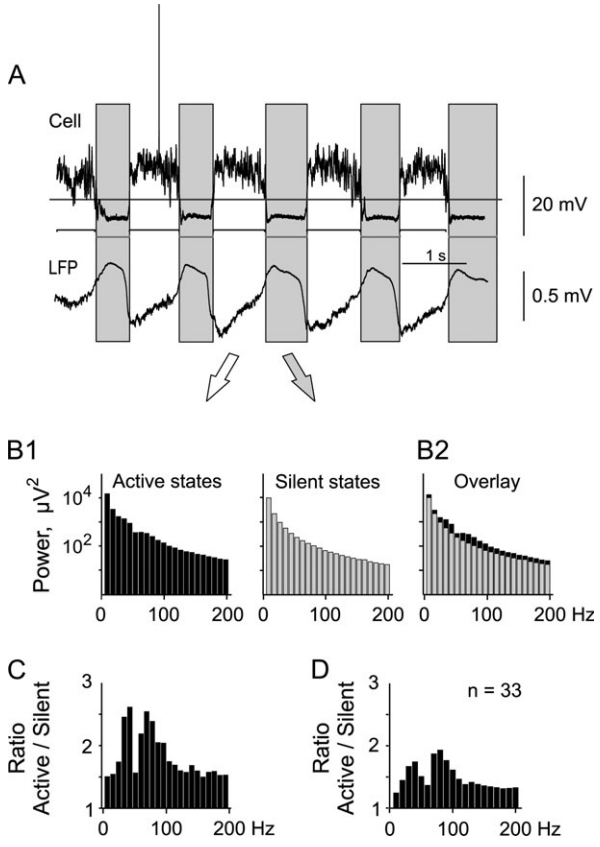

Figure 3. Comparison of power spectrum components in the LFP during the active and silent states in cells. (*A*) Simultaneously recorded membrane potential and LFP signals. Cell has clear active and silent states. The states were detected using a level shown as horizontal line. The detected active and silent states are shown with horizontal bars below the membrane potential trace. Large vertical gray bars mark periods of silent states in the cell. (*B*) Power spectra of the LFP during periods of the active and silent states in the cell (*B*1) and superposition of the 2 power spectra (*B*2). Power spectra are shown with bin width of 10 Hz. Ordinate scaling is logarithmic. Note that all components are smaller during the silent states but the difference is not uniform and depends on frequency. (*C*) Ratio of the corresponding power spectrum values during active and silent states, calculated for the data from (*B*). Note that the ratio is maximal in the range between 20 and 100 Hz. A trough around 60 Hz is due to the filtering used during the recording to reduce the contribution of the mains frequency. (*D*) Same as in (*C*), but averaged data for 33 cell–LFP pairs. Note that the difference between active and silent states is largest at 20–100 Hz.

Active and Silent States Differ by the Power of Fast Oscillations

Apart from the different levels of the mean membrane potential, the active and silent states also clearly differ by the strength of the membrane potential fluctuations in the high-frequency range, the fluctuations being noticeably stronger during the active states. The rapid fluctuations of the membrane potential reflect intensive synaptic bombardment and thus high level of activity in the thalamocortical networks. This difference in the level of network activity accounts for the terms "active" and "silent" states. Because the LFP signal also expresses periods, during which the strength of high frequency fluctuations is clearly different, we decided to exploit this feature for detection of active and silent states in the LFP.

To identify the frequency range in which the difference between active and silent states in the LFP is most pronounced, we first detected the states in a cell, and then used them as a reference for comparison of the respective parts of the field potential signal, which was recorded simultaneously to the cell. Clear bimodality of the membrane potential distribution allowed for a straightforward segregation of active and silent states in the reference cell, with the use of a level. The state separation level, shown as horizontal line in each intracellular trace in Figure 2*A*, was set into the depth of the trough between the 2 modes of the membrane potential distribution (oblique arrows to the right of distributions in Fig. 2*A*). Periods when the membrane potential was above that level were considered as active states, and periods during which the membrane potential was below this level were considered as silent states. To avoid interruptions of the states due to occasional, noise-driven crossings of the level, we introduced the following rules: a period is considered as a continuous state if the membrane potential was above the level for the active state (or below the level for the silent state) for more than 90% of the time. The tolerated less than 10% interruptions were accepted only within the state but not on its borders. Further, crossings of the level for periods shorter than 40 ms were not considered as a state or an interruption of a continuous state. Vertical arrows (1) and (2) in Figure 2*A* indicate such very short level crossings. This procedure allowed clear and secure separation of active and silent states in the membrane potential traces, as illustrated in Figure 2*A* for 2 simultaneously recorded cells and for several further neurons in the following figures.

After detecting the states in the membrane potential, we selected in the LFP signal all periods, which corresponded to the silent states in the simultaneously recorded reference cell (gray vertical bars in Fig. 3*A*), and calculated the cumulative power spectrum for these parts of the LFP. After applying the same procedure to the active states, we got 2 power spectra of the LFP: one for the periods of active states in the reference cell and one for the periods of silent states in the reference cell (Fig. 3*B*1). An overlay of these 2 power spectra shows that in all analyzed frequencies from 10 to 200 Hz, the power of the LFP signal was higher during the periods when the reference cell was in active states (Fig. 3*B*2). Calculation of the ratio between these 2 power spectra (Fig. 3*C*) shows that the difference was most pronounced for the frequencies in the high–beta-gamma range (20–100 Hz; the trough around 60 Hz is due to filtering used to reduce the contribution of the mains frequency during the recording). Averaged data from 33 pairs of simultaneously recorded LFP and intracellular potential show consistency of

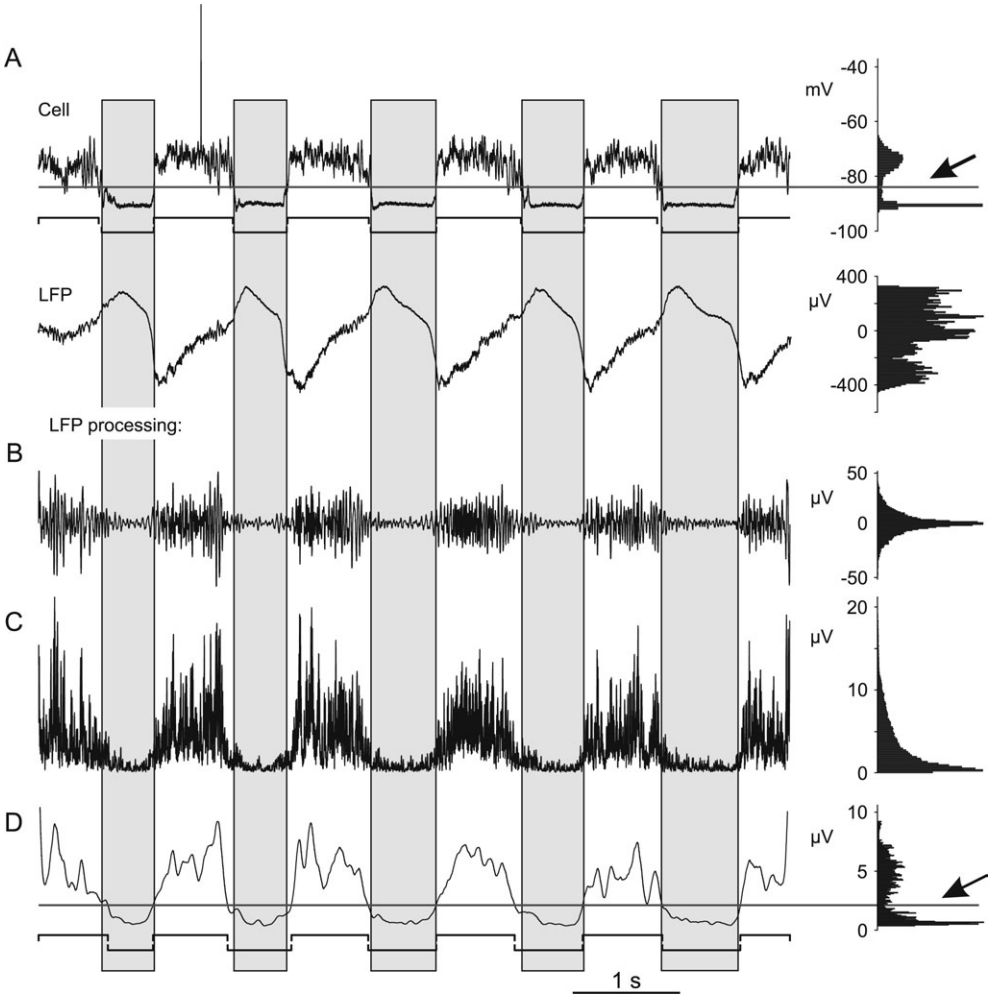

Figure 4. Processing of the LFP signal for detection of active and silent states. Simultaneously recorded membrane potential and LFP signal (*A*) and sequential steps of the LFP processing (*B–D*). (*A*) Simultaneously recorded membrane potential and LFP signal. Oblique arrow shows a gap in the bimodal distribution of the membrane potential. Horizontal line shows the level for separation of active and silent states in the membrane potential trace. Active and silent states in the cell are marked with horizontal bars below the membrane potential trace. Gray vertical bars mark periods of silent states in the cell. Histograms on the right-hand side show distributions of membrane potential and LFP signal (*A*) or processed LFP (*B–D*). (*B*) Extraction of the frequency components, which are most different between active and silent states, by band-pass filtering in the range 20–100 Hz. (*C*) Standard deviation of the filtered LFP calculated in a running window of 5-ms length. This operation is equal to root mean square in this case. (*D*) Linear filtering (50 ms frame) of the signal from (*C*). The distribution of the processed signal is clearly bimodal; the oblique arrow shows the gap between the modes. The horizontal line shows the level, which was used to separate active and silent states. Detected states are shown with horizontal bars below the trace. Note that the states detected in the LFP correspond, with little deviations, to the states detected from the intracellular recording.

the difference between the LFP power during periods of active and silent states in the 20- to 100-Hz band, with the mean ratio of 1.69 ± 0.75 (Fig. 3*D*). For the frequencies higher than 20 Hz, the difference in the LFP power during periods of active and silent states in the cells was highly significant ($P < 0.001$).

Processing of the LFP for the Detection of Active and Silent States

Because the most pronounced difference in the LFP signal between periods of active and silent states in the reference cell was found for the frequencies between 20 and 100 Hz, we selected this component of the LFP signal for the further analysis. The lower bound was selected for 2 reasons: 1) because of the high significance ($P < 0.001$) of the power difference during active and silent states and 2) because lower frequencies, having periods longer than 50 ms, could have compromised the temporal precision of detection of individual episodes of activity or silence. The upper bound was set at 100 Hz because higher frequencies contribute only little to the power during nonparoxysmal oscillations (Grenier and others 2003). The 20- to 100-Hz band contained 75.5 ± 20% of the total power above 20 Hz, whereas frequencies between 100 and 200 Hz contributed only 4.8 ± 3.6% ($n = 11$).

The state detection procedure in LFP consisted of the following steps. First, the 20- to 100-Hz component was extracted by performing fast Fourier transformation (FFT) of the signal, then setting in the result all coefficients, which corresponded to frequencies below 20 Hz and above 100 Hz to zero, and then performing an inverse FFT (see Volgushev and others 2003). In this component of the LFP signal, the amplitude of the fluctuations was clearly correlated with the states in the reference cell, stronger fluctuations occurring during active states and weaker during the silent states (Fig. 4*A*,*B*). In the second step, we processed the filtered signal to accentuate the difference between the periods of high-amplitude fluctuations and those of low amplitudes. We calculated the standard

deviation (which in this case is equal to the root mean square) of the filtered signal in a running frame of 5 ms (Fig. 4*C*). The resulting trace in Figure 4*C* shows a clear correlation with the membrane potential trace (Fig. 4*A*, cell). This similarity increases further after smoothing the obtained trace with a 50-ms running frame linear filter (Fig. 4*D*; see Fig. 6 and related text for the procedure used to optimize the length of the running frames). The signal, obtained after application of the above procedures to the LFP, will be referred to as "processed LFP" in the following text. The amplitude distribution of the processed LFP signal becomes bimodal, and a separation-by-the-level principle could be applied.

In the last step we separated active and silent states, placing the level at the local minimum in the gap between the 2 peaks in the amplitude distribution of the processed LFP signal (Fig. 4*D*). The local minimum in the distribution was detected using an automatic algorithm. This formal algorithm was developed to match the results of the expert estimation and consisted of the following steps. First, we cut 5% of the values with highest amplitudes in order to exclude spurious extremities. Then a 100-bin distribution was constructed from the remaining 95% of the values. The data were segregated into 3 clusters by their amplitude using K-Means Clustering procedure of MatLab. The cluster with the lowest center reliably contained the distribution peak at low amplitudes, corresponding to the silent states. In the next step, the algorithm searched for a local minimum between the center of this low-amplitude cluster and a limit set at 50% of data sorted by the amplitude. The 50% limit was reliably located on the ascending slope of the broad peak in the amplitude distribution, corresponding to the active states. During the search for the local minimum, 3 adjacent bins were averaged. The level for state separation was then set at this minimum. The active and silent states were separated using this level and applying the same rules (90% of state above/below the level and 40-ms minimal length—see above) as used for the detection of active and silent states in the membrane potential.

The active and silent states detected with this method in the LFP are in good correspondence to the active and silent states of the membrane potential in the simultaneously recorded reference cell (compare Fig. 4*A*, cell, and Fig. 4*D*). It should be noted here that such a clear threshold segregation of the LFP signal into periods that correspond to active and silent states in the simultaneously recorded reference neuron becomes possible only after the described processing (Fig. 4*D*). In the multimodal distribution of the nonprocessed LFP signal (Fig. 4*A*), it is clearly not possible to set a level, which would correspond to transitions between the states in the reference cell.

Quantification of State Correspondence: Coincidence Index

Despite an overall good correspondence between the states detected in the membrane potential and in the LFP, their overlap is not perfect. To estimate the quality of state detection by our method, dependence of its performance on variation of recording techniques, and related questions, we introduced a numeric "coincidence index (CoIn)", which provides a quantitative measure for the degree of overlap in the occurrence of states in several signal channels. Let *X*, *Y*, *Z*, . . . be the sequences of states, either active or silent, which occur in each of several simultaneously recorded cells or LFP signals. Total length of the states in each sequence is LX, LY, LZ, ... The index is then calculated as the ratio (in percent) between the time of intersection of the states in all channels and the mean of the total length of states in each sequence:

$$\mathrm{CoIn} = \mathrm{Intersection}(X, Y, Z, \ldots)/\mathrm{Mean}(\mathrm{LX}, \mathrm{LY}, \mathrm{LZ}, \ldots) \times 100\%.$$

The CoIn can take values between 0% and 100%, it can be computed for 2 or more channels and is insensitive to permutations of the channels. It depends only on the length of states and their relative timing but not on the total length of recording. Figure 5 illustrates the calculation of the CoIn between 2 channels for 3 hypothetical cases. In each of the cases, the length of the states in the 2 channels does not change but the relative timing of the states varies. In the case of Figure 5*A*, with partial, complete, or no overlap of the states in the channels *X* and *Y*, CoIn is 60%. In the case of Figure 5*B* all states in the channel *Y* occur within the states of the channel *X*. However, because some parts of the states in *X* occur during periods of "not-state" in *Y*, CoIn is 80%, which is below its upper limit. This illustrates an important property of the index, its sensitivity to the nonoverlapping portion of the state sequences. The upper limit of the CoIn (100%) would be reached only in a case of complete identity of the 2 sequences of states (not shown). Presence of a nonoverlapping portion in any of the state sequences leads to diminishing of the CoIn. In a case when the states in channels *X* and *Y* do not overlap at all, the CoIn reaches its minimum at 0% (Fig. 5*C*).

For each set of simultaneously recorded LFP and intracellular activity of neurons, we first calculated the CoIn separately for active states ($\mathrm{CoIn_{up}}$) and silent states ($\mathrm{CoIn_{down}}$). Their mean,

$$\mathrm{CoIn_m} = (\mathrm{CoIn_{up}} + \mathrm{CoIn_{down}})/2,$$

was then taken as an overall quality index of the coincidence of states in the cell–LFP pair. For the example shown in Figure 4, the CoIns were $\mathrm{CoIn_{up}}$ = 86.3, $\mathrm{CoIn_{down}}$ = 79.9, and $\mathrm{CoIn_m}$ = 83.1.

We used the CoIn to address the following issues: 1) optimization of the parameters of the LFP processing for state detection, 2) estimation of the quality of the detection method, 3) investigation of the effects of variations in recording methods

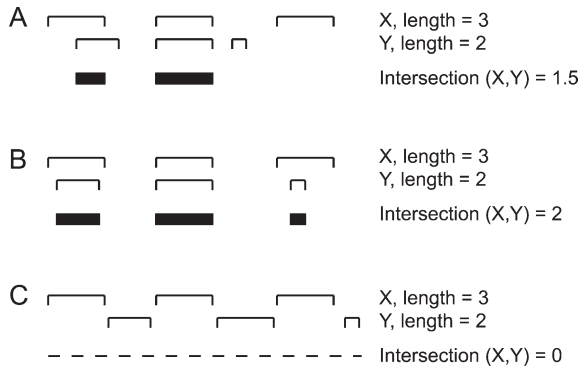

Figure 5. Calculation of CoIn for 3 pairs of hypothetical state sequences. In panel *A–C*, a pair of sequences of states (*X*, *Y*) and their intersection is shown. In the set *X*, each state has a length of 1. In the set *Y*, the length of the states is 0.75, 1, 0.25. The 3 examples in *A–C* differ by relative timing of the states. CoIns, calculated as the ratio of intersection to the mean length, are 60% in (*A*), 80% in (*B*), and 0% in (*C*).

and LFP filtering on the performance of the method, and 4) evaluation of possible reasons of small differences between the states detected in the LFP by our method and the states seen in the membrane potential traces of simultaneously recorded cells.

Optimization of Parameters of the LFP Processing

To optimize parameters of the LFP processing, the lengths of the running frames for calculation of the standard deviation and for smoothing the final trace (see above, Fig. 4, and related text), we used the following procedure. For 10 sets of data, each consisting of 2 intracellularly recorded cells and the LFP, we detected active and silent states in the LFP, while systematically varying the length of the frames. The length of the frame used for calculation of the standard deviation was set to 5, 10, 25, or 50 ms. The length of the smoothing frame was taken at least 2 times longer and was set to 10, 25, 50, or 100 ms. For each data set, active and silent states were detected in the LFP with different frame settings, and their CoIns with the states seen in the 2 simultaneously recorded intracellular traces were calculated. Results of this analysis are presented in Figure 6. The average of results from 10 data sets shows that the highest CoIn values were obtained when the standard deviation window was 5 ms and smoothing window 50 ms (Fig. 6*A*). The difference to the other settings is clear, albeit not big, in the range of few percent. For different sets of data, the highest CoIns were obtained with slightly different settings of the frames. With the frame settings corresponding to the peak in the averaged data plot (5 and 50 ms), also the deviation of the CoIns for the whole sample was minimal (0.56 vs. 1.43, 1.18, and 1.59 with other frame settings). It should be noted that the difference in CoIns obtained with the sample optimal and the optimal for a particular set of data was only minor, usually less than 2%. Based on these results, we used a 5-ms frame for calculation of the standard deviation and a 50-ms window for the smoothing in all further analyses.

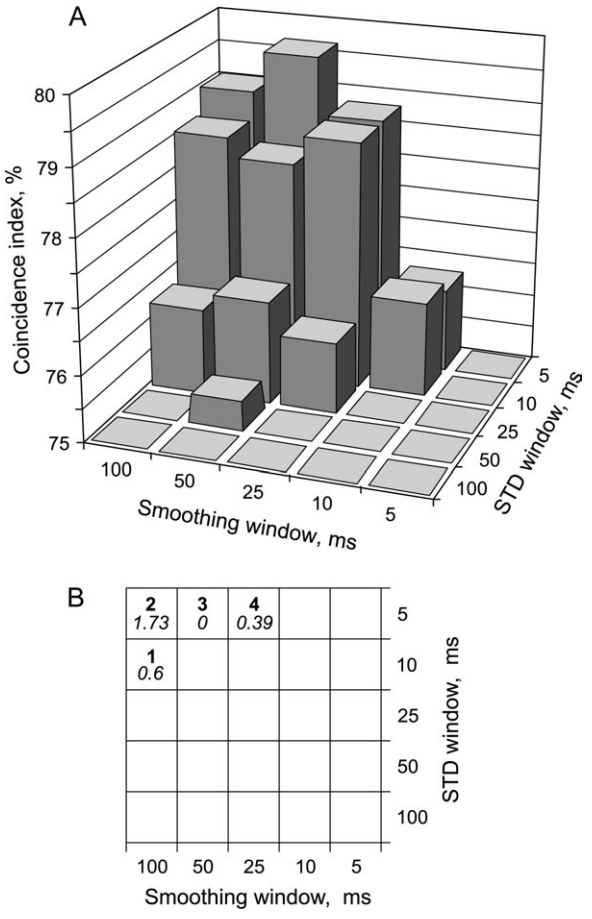

Figure 6. Dependence of the CoIn of the states in data sets consisting of 2 simultaneously recorded neurons and LFP on the length of frames used for calculation of standard deviation and for smoothing. With each combination of the length of the frames, the states were detected in the LFP, and their CoIns with the states in 2 simultaneously recorded cells were calculated. (*A*) Each bar shows averaged data for 10 data sets. The maximal CoIn and thus optimal detection of states in the LFP were obtained with a 5-ms frame for standard deviation and 50-ms frame for smoothing. (*B*) For each combination of frame lengths, the number of data sets, for which that combination gave maximal CoIn is shown (bold numbers) together with the mean deviation of the CoIns from those obtained with the sample optimal frames (italic numbers). Note that the CoIns, obtained with the sample optimal frames (5 ms, 50 ms), deviate by less than 2% from the optimal for each data set.

Estimation of the Quality of State Detection in the LFP

Next, we used the CoIn to estimate the quality of the detection of states in the LFP by our method. Detection of the states obviously depends on the setting of the level, which separates active and silent states. This dependence is quantified in Figure 7. With the level set too high, the length of the active states becomes underestimated and the length of the silent states overestimated (Fig. 7*B*, lower panel). When the level was set too low, the active states expand and their length is overestimated, and the silent states shrink and their length is underestimated (Fig. 7*B*, upper panel). We have varied the level systematically and calculated CoIns between the states, detected with the different level settings, and the states in the simultaneously recorded cell. The level, with which the states in the LFP signal showed maximal coincidence with the states in simultaneously recorded reference cell, is referred to as the optimal level. The graph in Figure 7*C* illustrates several important features of the dependence of the CoIns on the level setting. First, dependences of the CoIns, calculated both for the active states and silent states, as well as their mean, have broad hilltops, and the regions around their maxima are relatively flat. Second, the optimal levels, which give the highest CoIn between the states in the LFP and in the membrane potential, have very similar values for active and silent states. Finally, the optimal levels for all 3 CoIns lay in the trough of the amplitude distribution of the processed LFP signal, and thus the level found by the method as the local minimum in this trough, is located not far from the optimal value. In the example in Figure 7*A,C* the level found by the method differs by 0.2 μV from the optimal (Fig. 7*C*, inset, Level error). This led to only a minor difference between the CoIn of the states found in the LFP by our method and the best possible fit to the states seen in the membrane potential trace. The CoIns, calculated for the states found by the method, differed by as less as 0.37% from the optimal (Fig. 7*C*, inset, Index error). Also in other pairs of simultaneous intracellular and LFP recordings, the level found by the method deviated little from the optimal. As a result, the coincidence between the states in the LFP and in the membrane potential trace was also close to the maximal possible. Averaged level error was 0.25 ± 0.12 μV (n = 14), and averaged CoIn errors were Error($CoIn_{up}$) = –0.54 ± 0.85%, Error($CoIn_{down}$) = –1.4 ± 0.93%, and Error($CoIn_{m}$) = –0.98 ± 0.72%. Note that the errors of the CoIns are about 2 orders of magnitude lower than the values of the indexes.

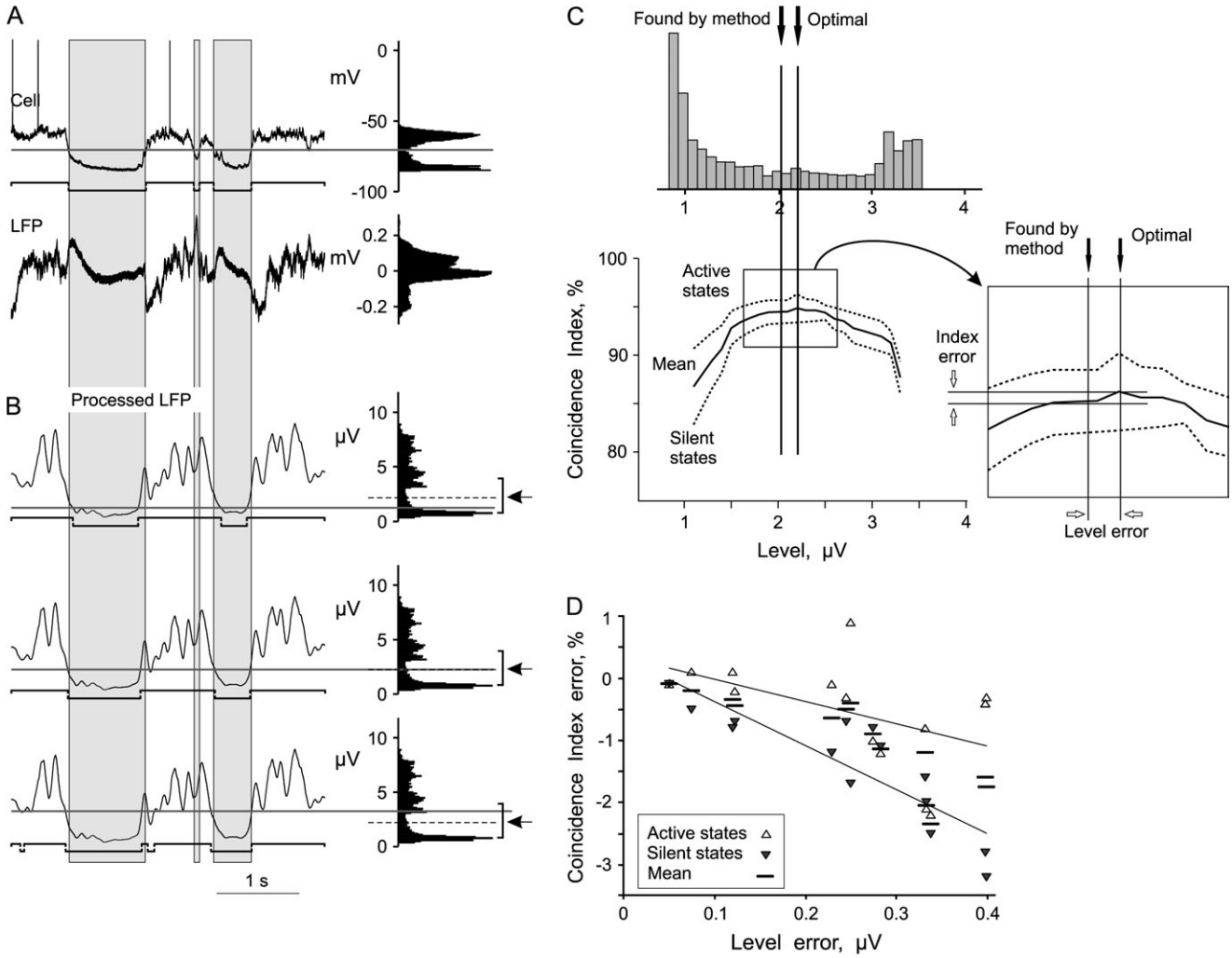

Figure 7. Estimation of the quality of detection of active and silent states in the LFP signal. (*A*) Simultaneously recorded membrane potential and raw LFP. In the membrane potential trace, solid horizontal line shows the level for the separation of active and silent states, which are marked with horizontal bars below the trace. Gray vertical bars mark periods of silent states in the cell. (*B*) Three traces of the LFP signal from (*A*), processed as described before. The 3 panels are identical except for the level used to separate active and silent states and the detected states. The level is indicated with a solid horizontal line, the detected states are shown below each trace. The level was set below the optimum (upper of the 3 panels, level at 1.2 μV), at the optimum (middle panel, level at 2.2 μV), or above it (lower panel, level at 3.2 μV), as indicated. Optimal level for state separation was found by optimization procedure, which maximized the mean of the CoIns ($CoIn_m$, coincidence of states in the LFP and in the cell) for active and silent states. In each of the 3 distributions, optimal level is shown with an interrupted line and an arrow. With the level set below the optimal, the active states got excessively enlarged and silent states shrunk (vice versa in case of the level set above the optimum). In either case the coincidence of the states found in the LFP with the states observed in the membrane potential decreases, leading to the smaller values of the CoIns. (*C*) Coincidence between the states in the cell and the LFP (CoIns) plotted against state separation level (results from the same data as in *A*, *B*). The part of the distribution of the potential values of the processed LFP signal, marked by the vertical bars to the right from distributions in (*B*) is shown above the plot, at the *X*-scale identical to that of the plot. In the plot, dependence of the CoIns between cell and LFP on the level setting is shown for active and silent states, $CoIn_{up}$ and $CoIn_{down}$ (dotted lines), and for the mean CoIn ($CoIn_m$) (solid line). Optimal level and the level found by the method are indicated with vertical lines and arrows. In the inset, "Level error" and "Index error" illustrate how the values for the plot in *D* were calculated. (*D*) CoIn errors (ordinate) plotted against level errors for 14 cell–LFP pairs. Upward-pointed triangle symbols: active states, downward-pointed triangles: silent states, mean: horizontal bars. Note that in all cases, the CoIns between the states in the cell and the states found in the LFP deviate from the optimum by less than 3%.

The above results show that our method can find in the LFP signal the active and silent states, which coincide almost optimally with the states seen in the membrane potential. The averaged CoIns, calculated for 14 pairs of simultaneous LFP and intracellular recordings, were 86.1 ± 4% for the active states, 76.6 ± 8.7% for the silent states, and 81.3 ± 5.6% for the mean. In all 14 cases, these values were below 95%.

Method Performance under Different Recording Conditions: Depth versus Surface EEG

Having established and formalized the basic procedure, which allows to segregate periods of active and silent states of the neural network by the analysis of the LFP signal, we set to test its performance with the LFP signals obtained under variable recording conditions. One factor, which influences critically the phase relation between intracellular activity and field potentials, is the positioning of the recording electrode relative to the surface of the cortex (Speckmann and Elger 2005). So far, we have used for our analysis the field potentials, recorded with an electrode inserted into the neocortex to a depth of about 1 mm, "depth" LFP or EEG. We wanted to test if our method of state detection will also work with signals recorded from the electrodes located at the cortical surface, "surface" LFP or EEG. To this end, we made simultaneous intracellular recordings and field potential recordings with 2 electrodes, one electrode inserted into the cortex and one positioned at the cortical

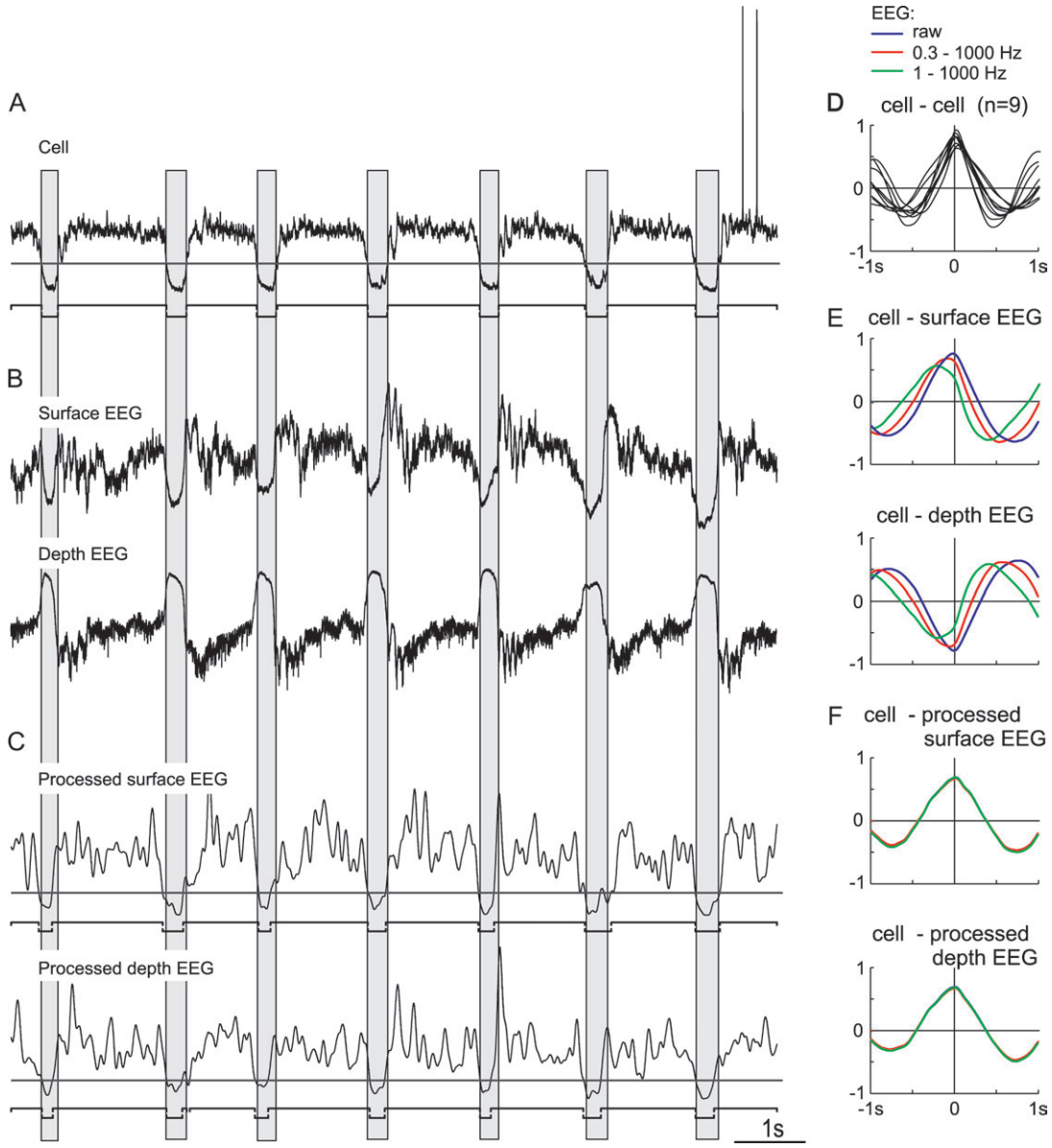

Figure 8. Detection of active and silent states from the EEG recorded with surface and depth electrodes and their relation to the states in the intracellularly recorded neuron. (*A*) Membrane potential trace. Active and silent states in the cell are marked with horizontal bars below the trace; horizontal line shows level for their separation. Gray vertical bars mark periods of silent states in the cell. (*B*) Surface and depth EEG recorded simultaneously with the cell in (*A*). Note a nearly contraphase relation between the surface and depth EEG. As a result, the slow waves of the membrane potential in the cell in (*A*) are inphase with the surface EEG but in contraphase to the depth EEG. (*C*) Processed surface and depth EEG (see Fig. 4*B–D* for details of the processing). Horizontal lines show levels for the separation of active and silent states. Active and silent states are marked with horizontal bars below the traces. Note that the states detected in both surface and depth LFP corresponds, with little deviations, to the states detected from the membrane potential recording. (*D*) Correlation between membrane potential changes in pairs of simultaneously recorded cells. Cross-correlograms for 9 pairs are superimposed. Note positive correlation with little phase shift in all 9 pairs of cells. (*E*) Correlation between membrane potential changes in a cell and the EEG, recorded simultaneously with surface or depth electrodes. The correlograms, computed between membrane potential and raw EEG (blue) and filtered EEG (red and green, band-pass filtered as indicated) are shown superimposed. Note that 1) slow waves in the intracellular activity are in phase with the surface EEG, but in contraphase to the depth EEG, and 2) the phase shift between the intracellular activity and the EEG depends on filtering. (*F*) Correlation between membrane potential changes in a cell and processed surface and depth EEG, raw or filtered. Same data as in (*B*) were used. The blue, red, and green correlograms are superimposed and overlap almost completely. Note that the phase relation between the EEG processed with our method and intracellular activity remains the same, irrespective of the location of the recording electrode (surface or depth EEG recording) and filtering of the EEG.

surface. The surface EEG has, apart from a lower amplitude, a nearly contraphase relation to the depth EEG (Fig. 8*B*) and thus these 2 signals have an opposite phase relation to changes of the membrane potential in a simultaneous intracellular recording (Fig. 8*A*). However, after being subject to our processing procedure, the resulting "processed" signals express a similar pattern of the amplitude changes (Fig. 8*C*). This pattern of slow changes, which is now common for both, processed depth EEG and processed surface EEG, also clearly corresponds to the slow pattern of the hyper- and depolarization states of the membrane potential in the simultaneously recorded cell (Fig. 8*C*,*A*). Moreover, amplitude distributions of the processed LFP signals have clear modes (not shown), allowing secure level setting and separation of active and silent states (Fig. 8*C*). The states, detected by our method in the surface and in the depth EEG, are in good correspondence to each other and to the active and silent states seen in the reference neuron (Fig. 8*A–C*). Thus, our method can reliably detect active and silent states in

the EEG signals, recorded from the electrodes located inside the cortex or atop the cortical surface.

The above conclusions are substantiated by the results of correlation analysis (Fig. 8*D–F*). Cross-correlation between the membrane potential changes in pairs of simultaneously recorded cells is characterized by a broad positive peak, centered at about zero, and flanked by the negative troughs. Both, the positive peak and the negative troughs are symmetrical. This general shape of the correlation function is typical for different cell pairs, as illustrated in Figure 8*D* that shows superposition of the correlation functions of the membrane potentials for 9 pairs of cells. In contrast to the uniformity of the shape of cell–cell correlation, the correlation between the membrane potential and the LFP signal may be very different and varying from one pair cell–LFP to the other, as demonstrated already in early studies (Klee and others 1965; Creutzfeldt and others 1966). For the correlation between the membrane potential and the surface EEG, a broad positive peak is typical (Fig. 8*E*, upper panel). Both the amplitude of the main peak and its shift from zero are strongly affected by filtering of the EEG. In the example shown in Figure 8*E*, filtering of the EEG with 0.3- to 1000-Hz or 1- to 1000-Hz band-pass filters results in reduction of the amplitude of the main peak (from 0.77 for correlation with the raw EEG to 0.7 and 0.58, respectively) and to a change of its location from –13 to –80 ms and –230 ms, respectively. Correlation between the membrane potential and depth EEG is characterized by a broad negative peak (Fig. 8*E*, lower panel). Also for the depth EEG, filtering has a pronounced effect on both the amplitude and position of this main negative peak. However, after the EEG is processed as outlined above, its correlation to the changes of the membrane potential becomes very similar to the correlation seen in cell pairs. Irrespective of whether a depth or surface EEG was used, the correlation function between the processed EEG and the membrane potential in the reference cell is symmetrical, with the peak located around zero (Fig. 8*F*). Moreover, the correlation function between the processed EEG and the membrane potential of the reference cell becomes insensitive to the filtering applied to the EEG signal before the processing, as demonstrated by an almost complete overlap of the blue, red, and green correlation functions in Figure 8*F*. Population analysis showed that the correlations in pairs cell–LFP were weaker and showed higher variability in the absolute value and location of the main peak than correlations in the pairs cell–cell or cell–processed LFP. In cell–LFP pairs, the mean absolute value of correlation peak was 0.41 ± 0.14, as compared with 0.79 ± 0.09 or 0.64 ± 0.05 in cell–cell and cell–processed LFP pairs ($P < 0.001$, $n = 9$). The position of the peak was highly variable in pairs cell–LFP, 295 ± 143 ms, both the average value and the variance significantly higher ($P < 0.001$ for all comparisons) than in pairs cell–cell (19 ± 15 ms) or cell–processed LFP (15 ± 18 ms). These data show that 1) although the correlation between the raw LFP signal and changes of the membrane potential in individual cells is usually strong, it is highly variable in magnitude and peak shift or phase, and 2) with our processing we extract from the LFP signal those components that change in phase with the slow fluctuations of the membrane potential in neurons between the active and silent states.

Method Performance under Different Recording Conditions: Prefiltering of the LFP

Another parameter, which varies widely in different LFP/EEG studies, is filtering of the signal. Most often, a band-pass filter composed of 2 one-pole filters is used during the recording of the LFP or EEG, with the high-pass cutting frequency varying in the range from 0.1 to 1 Hz and low-pass cutting frequency in the range 100–1000 Hz but occasionally even at 30 Hz. To study the effect of filtering the LFP signal on its relation to the intracellular activity, we compared changes of the membrane potential in neocortical neurons with the LFP, either raw or filtered off-line with different settings of the band-pass filters. This analysis confirms the above results of correlation analysis, demonstrating that filtering of the LFP signal modifies its phase relation to the underlying intracellular activity (Fig. 9). Increasing the high-pass cutting frequency from 0.1 to 1 Hz leads to a clear phase advancing of the peaks in the LFP signal with respect to the beginning of the silent or active states in the reference cell. Comparison of black, green, and blue traces in Figure 9 illustrates this effect. Superposition of the LFP signals (Fig. 9*E*, upper traces) filtered with different settings of the band-pass filter makes also clear that results of state detection in the LFP, if obtained with the use of any procedure exploiting the amplitude level of the unprocessed LFP signal, would be severely affected by the filtering. This conclusion is substantiated by comparison of the amplitude distributions of the corresponding filtered LFP signals. Filtering affects the degree of skewness and the width of the distributions, but neither of the distributions expresses clear bimodality, which would be a necessary precondition for a reliable setting of the level. One further effect, which becomes clearly apparent even after a mild high-pass filtering at 0.3 Hz, is a variable location of the peaks in the LFP within the periods of silent states in the reference cell. For example, during the silent state 1, the LFP peak is at about the middle of the state in the cell, whereas during the silent states 2 and 4 the LFP peak occurs toward the end and at the beginning of the state in the cell, respectively (Fig. 9, green and blue traces). Therefore, although peaks in the LFP did reliably occur during the silent states in the cells and thus could be used as a mark for the silent, hyperpolarized state of the neocortical neurons, it is not possible to tell whether at the LFP peak the neurons are in the beginning or in the end of the silent state.

Next, we have applied our method of state detection to the raw and to the filtered LFP signals and compared the results with the states detected in the intracellular recording of the reference cell. An intracellularly recorded neuron expressed unambiguous active and silent states, which are reliably segregated by the level set in the trough between the 2 modes in a clearly bimodal distribution of the membrane potential (Fig. 9*A*). Our processing method applied to the raw LFP signal, detects active and silent states, which correspond well to the states observed in the reference cell (Fig. 9*A,B*). Despite the pronounced effects of filtering on the shape of the LFP signal and its relation to the membrane potential changes in a reference cell, our method reliably detects active and silent states also in the filtered LFP (Fig. 9*C,D*). Notably, each processed LFP, either filtered or not, has an amplitude distribution with a clear gap, which allows unambiguous setting of the level and separation of the active and silent states (Fig. 9*B2–D2*). The results of state detection in the raw and in the filtered LFP signal with our method are in good correspondence to each other and to the states of the reference cell (Fig. 9*F*). Therefore, our method reliably detects active and silent states from the LFP signal, and the results of detection are affected little by prefiltering of the LFP signal with settings of band-pass filters that are commonly used during the recording.

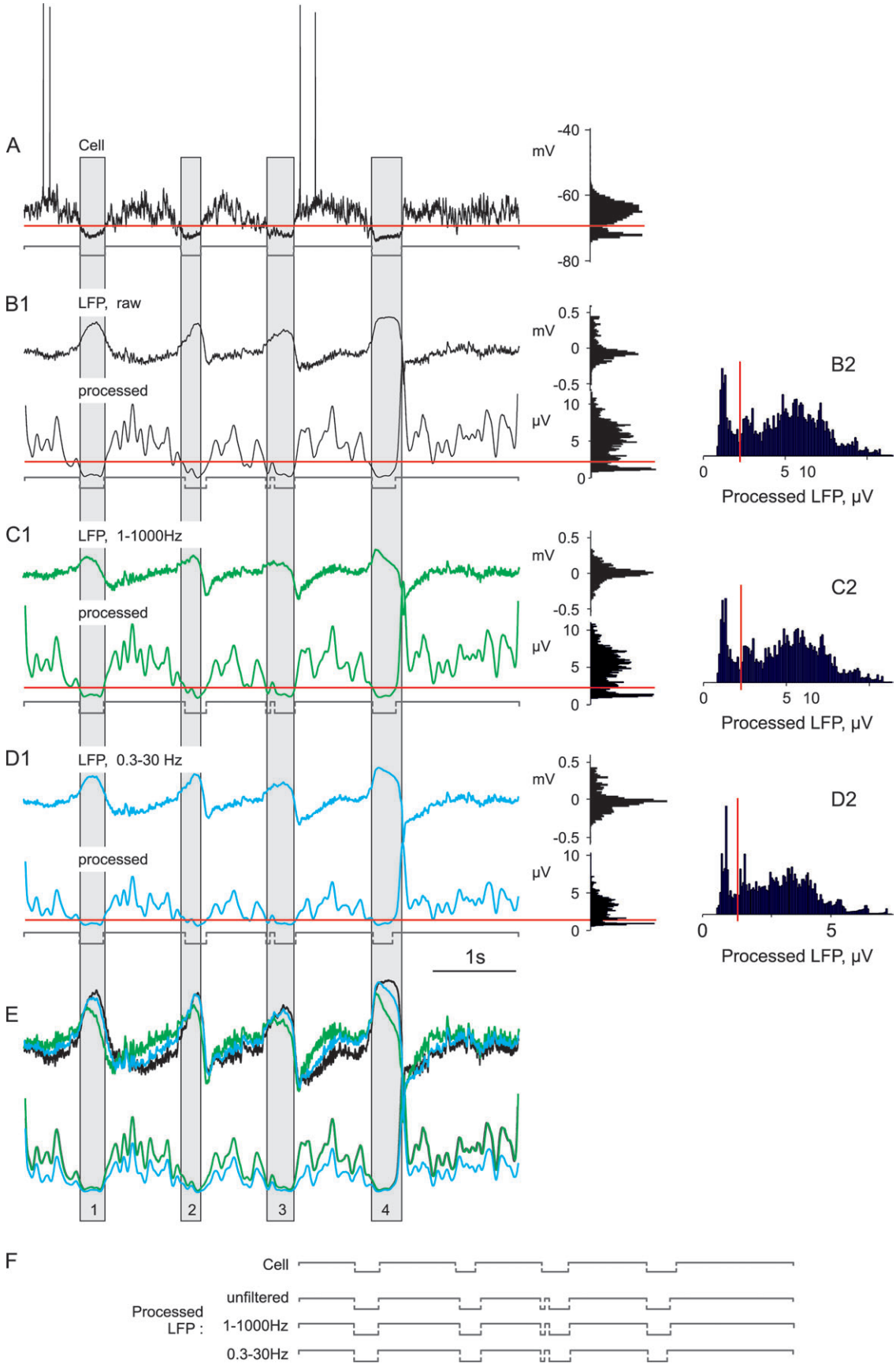
A
Cell
mV
-40
-60
-80
B1
LFP, raw
processed
0.5
mV
0
-0.5
10
μV
5
0
B2
0
5 10
Processed LFP, μV
C1
LFP, 1-1000Hz
processed
C2
D1
LFP, 0.3-30 Hz
processed
D2
5
1s
E
1
2
3
4
F
Cell
Processed LFP :
unfiltered
1-1000Hz
0.3-30Hz

To assess quantitatively the effect of the LFP filtering on the performance of our method of state detection, we did the following analysis. We used data-sets, consisting of the simultaneously recorded intracellular activity of 2 cells and the LFP. In these data-sets, we detected the states using the non-filtered LFP signal, and then after different pre-filtering of the LFP. For the pre-filtering, we used band-pass filter settings which are common in the LFP or EEG studies: 0.3–1000Hz, 1–1000Hz. In addition, we used an extremely narrow filter setting, often used in the clinical EEG recordings, 0.3–30 Hz (e.g., Schimicek and others 1994). After detecting the states in all 4 "versions" of the LFP, we calculated their CoIns with the states detected in the 2 simultaneously recorded cells. Figure 10 presents results of this analysis for 11 data sets. Data obtained from each data set are connected by the line. The results demonstrate that in most of the cases performance of the method was little affected by commonly used filtering, between 0.3 or 1 Hz and 100 Hz. Only the filtering in the 0.3- to 30-Hz band decreased the coincidence of the states detected in the LFP and those seen in the cells. However, even after this most severe filtering, CoIn changed by few percent only, indicating that the detected states were still in good correspondence to the periods of activity and silence in cells.

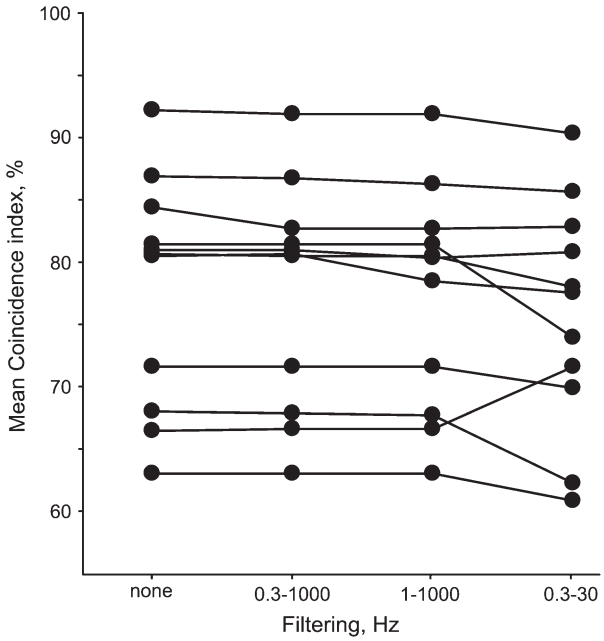

Figure 10. Effect of prefiltering on state detection in the LFP signal, and coincidence of the detected states with the states in 2 simultaneously recorded neurons. In each data set, consisting of 2 simultaneously recorded neurons and LFP, active and silent states in the LFP were detected 4 times: in a raw LFP signal, and after prefiltering, as indicated. The CoIns of detected states with the states in 2 simultaneously recorded cells were then calculated. Data for 11 data sets; results for each data set are connected with a line.

Factors Contributing to Variability in State Coincidence

One further point, revealed by the results presented in Figure 10, is high variability in the coincidence coefficients and thus variable degree of correspondence between states detected in cells and in the LFP among different sets of data. Two possible reasons may have contributed to this variability and led to the subtle differences between the states detected in the cells and in the field potentials: 1) errors of our detection method and 2) the intrinsic variability of neuronal activity. To compare the relative contribution of these 2 factors, we used data sets with simultaneously recorded LFP and 2 or more intracellular recordings. From these data sets, we composed cell–LFP and cell–cell pairs and compared the state CoIns calculated for these pairs. Because detection of the states from the membrane potential traces is unambiguous, CoIns in cell–cell pairs reflected the intrinsic variability in the data, and were free from detection errors. The CoIns in cell–cell pairs were 87 ± 7.9% for the active states, 80.8 ± 12.5% for the silent states, and 83.9 ± 9.7% for the mean ($n = 24$). In the cell–LFP pairs, the CoIns were slightly higher (Fig. 11*A*, active: 89 ± 5.6%, silent: 81.7 ± 8.2%, mean: 85.4 ± 5.8%). Moreover, the CoIns in simultaneously recorded cell–cell and cell–LFP pairs showed high and significant correlation (Fig. 11*A*, active states: $r = 0.74$, silent states: $r = 0.82$, both active and silent states: $r = 0.81$, $P < 0.001$ for all correlations). The significant correlation between the CoIns and an overall correspondence of the state coincidence in the simultaneously recorded cell–cell and cell–LFP pairs show that the intrinsic variability of neuronal data and differential precision of synchronization of the slow waves in the neural network could account for the large part of variability in the coincidence of the silent and active states, seen in different recordings.

A possible correlate of the differential precision of the activity synchronization in the neuronal network during the slow waves is the relative contribution of the low-frequency components (<4 Hz) to the total power of the LFP signal. To assess the contribution of this factor to the variability of the coincidence between the states in the LFP and intracellular recordings, we plotted the CoIn in pairs cell–LFP against the ratio of the LFP power below 4 Hz and above 4 Hz (Fig. 11*B*). With the stronger contribution of the low-frequency components to the LFP power, indicative of the higher synchronization of network activity, the coincidence between states detected in the LFP and those seen in the intracellular recordings increased and the variability of the coincidence among different data decreased. Moreover, CoIns for both active and silent states showed significant correlation with the power ratio ($r = 0.43$, $P = 0.018$, for active states; $r = 0.65$, $P < 0.001$, for silent states; and $r = 0.66$, $P < 0.0001$, for the mean CoIn). These results substantiate the above conclusion that intrinsic variability of network functioning contributes significantly to the observed variability of state coincidence in different sets of data.

Figure 9. Detection of active and silent states in the filtered LFP signals, and their comparison with the states in a cell. Traces of the simultaneously recorded membrane potential in a neocortical neuron (*A*), LFP (*B*1), and filtered LFP (*C*1, *D*1). Below each LFP trace (*B*1–*D*1), processed signal with the level for state separation (horizontal line) and detected active and silent states (horizontal bars below the trace) are shown. Gray vertical bars in (*A*–*E*) mark periods of silent states in the cell. Histograms on the right-hand side show distributions of the potential values from the corresponding traces. (*B*2–*D*2) show distributions of the processed LFP signal with the levels for state detection at expanded scale and below each other to facilitate the comparison. (*E*) Superposition of the 3 unprocessed (upper) and processed (lower) LFP traces from (*B*–*D*), at expanded *Y*-scale. Note that filtering introduces a phase shift to the LFP signal and changes its phase relation to the slow waves in the membrane potential trace. In the processed LFP signal, filtering changes only the amplitude but not the phase relation to the membrane potential waves. (*F*) Sequences of active and silent states, as detected in the cell, unfiltered LFP, and in band-pass filtered LFP. Note that the states detected by our method in the filtered LFP correspond well to the states found in both, the intracellular recording and the raw LFP signal.

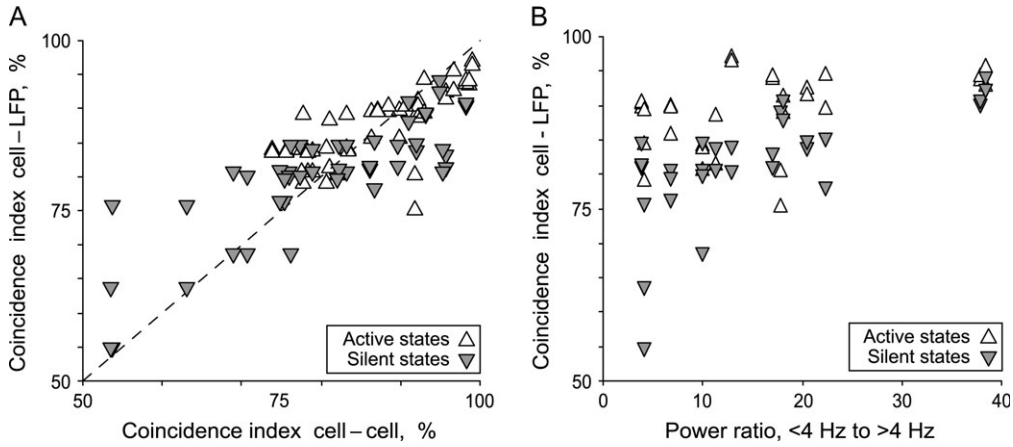

Figure 11. Factors contributing to the variability of the coincidence between the states detected in the LFP signal and those seen in neurons. (*A*) Coincidence of active and silent states in pairs cell–cell and cell–LFP. For this plot, data from 2–3 simultaneously recorded cells and the LFP signal were used, allowing to compose several pairs. Each point shows data for simultaneously recorded pairs cell–cell (abscissa) and cell–LFP (ordinate). Note correlated changes of the CoIns between pairs cell–LFP and cell–cell. (*B*) Dependence of the state coincidence in cells and in the LFP on the spectral composition of the LFP signal. Note that with increasing power of the low-frequency components in the LFP, the coincidence between states in cells and LFP increases and its variability decreases. Upward-pointed triangles: data for the active states; gray downward-pointed: data for the silent states.

Discussion

We have demonstrated that in neocortical cells, periods of activity and silence, which alternate during SWS (Steriade, Amzica, and Contreras 1996; Steriade, Contreras, and others 1996; Steriade and others 2001), can be quantitatively distinguished by the differential strength of fast, beta-gamma–band (20–100 Hz) fluctuations in the field potential. Exploiting this difference, we developed a new method of LFP analysis, which allows robust and reliable detection of active and silent states in neocortical cells during SWS. For the detection of the different states, either depth or surface EEG can be used. Moreover, the results of detection are affected little by prefiltering of the LFP.

Our method of detection of active and silent states in the neocortical network is based on the spectral difference of the LFP signal during neuronal activity and silence. The dependence of the spectral composition of the underlying signals, which are membrane potential changes in neocortical cells, on the state of neural network has been seen in various systems and conditions. Fluctuations of the membrane potential at frequencies >20 Hz increase in strength during active states of the SWS in the neocortex (Steriade and others 1991a; Steriade, Amzica, and Contreras 1996; Steriade, Contreras, and others 1996), during active states in striatal neurons (Stern and others 1997, 1998), and during depolarization phases of responses to sensory stimulation (Volgushev and others 2003). The occurrence of spindles (8–15 Hz) and beta-band fluctuations (15–25 Hz) in the EEG or intracellular activity is correlated with the phase of the slow, <1-Hz, EEG oscillations (Steriade, McCormick, and Sejnowski 1993; Steriade, Nunez, and others 1993a, 1993b; Contreras and Steriade 1995; Mölle and others 2002). Also in the EEG recorded during sleep in neurologically normal humans or patients with epilepsy, correlation between the phase of slow, <0.5-Hz, oscillations and the strength of fast EEG activities (Vanhatalo and others 2004), as well as covariance of the degree of coherence in a wide range of frequency components of the EEG (Bullock and others 1995), were observed. Taken together, these data are indicative of the intrinsic relation among EEG fluctuations at different frequencies. Our quantitative analysis of the frequency composition of the LFP signal during active and silent states supports this notion and extends the earlier observations. We show that the difference between active and silent states of the cortical network is expressed in the LFP most strongly and consistently in the frequency range of 20–100 Hz. The finding that high-frequency, around 100 Hz, LFP components are expressed stronger during active states, and thus should be accounted for when detecting the states and is essential for improving the precision of detection. Evidently, with increasing frequency, the temporal resolution increases as well. This provides a further argument for the use of a full-band EEG recording instead of severely filtered, 0.5- to 50 Hz, "routine clinical EEG" (see Vanhatalo and others 2005, for review).

Simultaneous intracellular recordings from 2–3 cells in line with the LFP signal gave us a unique possibility to assess the quality of our detection method by the direct comparison of the coincidence of active and silent states in cell–LFP pairs with the coincidence of states in cell pairs, in which the states in both channels were defined unambiguously by the membrane potential level. This analysis provided 2 lines of evidence, which prove the robustness and reliability of our detection method. First, coincidence of the states in cell–LFP pairs was of the similarly high level as the coincidence between the states in pairs of simultaneously recorded cells. Slightly higher coincidence in cell–LFP pairs could be due to the fact that the LFP signal, being an average of neuronal activity, has a reduced variability comparing with individual contributing cells. Second, separation of the active and silent states deviated only slightly from the best possible, as indicated by the low, less than 3% difference between the CoIns of the states detected by our method in the LFP and those observed in simultaneously recorded cells on the one hand and highest possible CoIns for that given data set on the other hand. Taken together, these results indicate that most of the variability of the coincidence between the states detected on the basis of the LFP and the states seen in the intracellular recordings can be attributed to intrinsic variability of neuronal network. Indeed, comparison of the slow fluctuations of the membrane potential in simultaneously recorded cells makes apparent that although essentially every cell is involved in the slow oscillation, not every neuron participates in every single cycle of the oscillation, and the onsets of active and silent states in any cell pair exhibit a certain

dispersion (Chauvette and others 2004; Volgushev and others 2004). As a result, even the active and silent states in simultaneously recorded cells do not coincide completely. One further supporting argument comes from the finding that the coincidence of states in simultaneously recorded cell–cell and cell–LFP pairs change in parallel, and the 2 measures show strong and significant correlation. This fact bears to the notion that the variable degree of synchronization of activity over the neural network, and the variable degree of involvement of any individual cell in that process, underlies the observed variability of coincidence between the states seen in individual cells and detected in the LFP.

In earlier studies, separation of the active and silent states of the neuronal networks has been made on the basis of the phase of the slow rhythm, whereby different criteria for detection of the states were used. The positive half-waves in the EEG were considered as periods of silent states, and the negative half-waves in the EEG as active states in cells (Contreras and Steriade 1995; Mölle and others 2002). In a recent study, the negative peaks in the scalp EEG were used as indicators of the transition from silent to active state (Massimini and others 2004). Our analysis demonstrates that although the correlation between the positivity/negativity in the EEG and the silent/active states of the neocortical network does exist and is usually strong, the phase relation between the slow component of the EEG and the beginning of the active and silent states in cells may vary, both in different cell–LFP pairs, but also for the same cell–LFP pair, when different episodes of the slow oscillation are compared. Even in episodes of slow waves, separated by just few seconds, the peak in the LFP may be located in the beginning, in the middle, or at the end of the silent state seen in the cell. Moreover, relative timing between the EEG peaks and beginning of the states in cells is highly sensitive to the filtering used during the EEG recording—the fact that complicates comparison of results of different studies. The algorithms of detection of states of the network on the basis of the phase of the slow EEG fluctuation face several more problems. When the peak in the EEG is not pronounced enough, the whole period of active or silent state escapes detection. Temporal precision of the detection is constrained by the low frequency, about 1 Hz or lower, of the signal components used. Our method, based on the analysis of the spectral composition of the LFP signal, including frequencies up to 100 Hz, overcomes these problems. It works well with either depth or surface EEG, is insensitive to prefiltering of the EEG during recording, and thus allows for a more robust and precise detection of both, occurrence of active and silent states, as well as their timing.

We would like to stress here that our method is aimed at the detection of the timing of each individual episode of activity and silence in the neocortical network during SWS. A precondition for the application of the method is the presence of the slow oscillations. Occurrence of the slow oscillations can be revealed with other methods, say those used for the identification of deep sleep (stages 3 and 4, see e.g., Niedermeyer 1999, for review).

Why separation of the silent and active states is important? Sleep is by no way a uniform state but consists of heterogeneous periods of brain activity. Sleep is important for memory consolidation (Maquet 2001; Steriade and Timofeev 2003; Huber and others 2004), whereby during different phases of sleep, traces of different types of memory, such as declarative or procedural, may be processed preferentially (Plihal and Born 1997). Also reactivity of the brain to external stimulation fluctuates during sleep dramatically and rapidly on the short timescale of seconds and hundreds of milliseconds. Recent data demonstrate that the amplitude and shape of the somatosensory-evoked potentials in humans critically depend on the phase of the slow EEG wave, at which the stimulus was applied. The amplitude of the evoked potentials progressively increases during the negative trend in the EEG, reaching wakeful values at about the negative EEG peak, and decreases well below the wakeful values during the positive trend in the EEG (Massimini and others 2003). According to the phase-guided definition of the states, as used by the authors (Massimini and others 2003), maximal responses were observed at the beginning of the active state. Different results were reported for the rat barrel cortex, where the postsynaptic responses, either subthreshold or leading to action potentials, were suppressed during the active states (Petersen and others 2003; Sachdev and others 2004). It remains to be clarified, if the above difference was due only to the very different subjects and experimental conditions or if problems in the detection of active and silent states of the cortical network may have contributed as well. Because our method allows for a more precise detection, on the basis of the LFP or EEG signal, of active and silent states of cortical network, it opens new possibilities to address these questions and to gain better understanding of the processes that take place during "active" sleep.

Notes

We are grateful to Sofiane Boucetta for participation in one experiment, to Marina Chistiakova for comments on the manuscript, and to Dimitrios Giannikopoulos for improving the English. Supported by the Canadian Institutes of Health Research (CIHR) grant MOP-37862, the Natural Sciences and Engineering Research Council of Canada grant 298475 to IT and the Deutsche Forschungsgemeindschaft SFB 509 TPA5 to MV. IT is a CIHR scholar. *Conflict of Interest*: None declared.

Address correspondence to Maxim Volgushev, Department of Neurophysiology, Ruhr-University Bochum, MA 4/149 D-44801 Bochum, Germany. Email: maxim@neurop.rub.de.

References

Antognini JF, Carstens E. 2002. In vivo characterization of clinical anaesthesia and its components. Br J Anaesth 89:156–166.

Blake H, Gerard RW. 1937. Brain potentials during sleep. Am J Physiol 119:692–703.

Bullock TH, McClune MC, Achimowicz JZ, Iragui-Madoz VJ, Duckrow RB. 1995. Temporal fluctuations in coherence of brain waves. Proc Natl Acad Sci USA 92:11568–11572.

Chauvette S, Boucetta S, Timofeev I. 2004. Origin of spontaneous active states in local neocortical networks during sleep oscillations. Society for Neuroscience Abstracts Program No. 638.6.

Contreras D, Steriade M. 1995. Cellular basis of EEG slow rhythms: a study of dynamic corticothalamic relationships. J Neurosci 15:604–622.

Creutzfeldt OD, Watanabe S, Lux HD. 1966. Relations between EEG phenomena and potentials of single cortical cells. II. Spontaneous and convulsoid activity. Electroencephalogr Clin Neurophysiol 20:19–37.

Crochet S, Chauvette S, Boucetta S, Timofeev I. 2005. Modulation of synaptic transmission in neocortex by network activities. Eur J Neurosci 21:1030–1044.

Grenier F, Timofeev I, Steriade M. 2003. Neocortical very fast oscillations (ripples, 80–200 Hz) during seizures: intracellular correlates. J Neurophysiol 89:841–852.

Huber R, Ghilardi MF, Massimini M, Tononi G. 2004. Local sleep and learning. Nature 430:78–81.

Klee MR, Offenloch K, Tigges H. 1965. Cross-correlation of electroencephalographic potentials and slow membrane transients. Science 147:519–521.
Mahon S, Deniau J-M, Charpier S. 2001. Relationship between EEG potentials and intracellular activity of striatal and cortico-striatal neurons: an in vivo study under different anesthetics. Cereb Cortex 11(4):360–373.
Maquet P. 2001. The role of sleep in learning and memory. Science 294:1048–1052.
Massimini M, Huber R, Ferrarelli F, Hill S, Tononi G. 2004. The sleep slow oscillation as a traveling wave. J Neurosci 24:6862–6870.
Massimini M, Rosanova M, Mariotti M. 2003. EEG slow (~1 Hz) waves are associated with nonstationarity of thalamo-cortical sensory processing in the sleeping human. J Neurophysiol 89:1205–1213.
Mölle M, Marshall L, Gais S, Born J. 2002. Grouping of spindle activity during slow oscillations in human non-rapid eye movement sleep. J Neurosci 22:10941–10947.
Niedermeyer E. 1999. Sleep and EEG. In: Niedermeyer E, Lopes da Silva FH, editors. Electroencephalography: basic principles, clinical applications and related fields. Philadelphia, PA: Lippincott Williams & Wilkins. p 193–207.
Olbrich E, Achermann P. 2005. Analysis of oscillatory patterns in the human sleep EEG using a novel detection algorithm. J Sleep Res 14:337–346.
Petersen CCH, Hahn TTG, Mehta M, Grinvald A, Sakmann B. 2003. Interaction of sensory responses with spontaneous depolarization in layer 2/3 barrel cortex. Proc Natl Acad Sci USA 100:13638–13643.
Plihal W, Born J. 1997. Effects of early and late nocturnal sleep on declarative and procedural memory. J Cogn Neurosci 9:534–547.
Rosanova M and Timofeev I. 2005. Neuronal mechanisms mediating the variability of somatosensory evoked potentials during sleep oscillations in cats. J Physiol 562.2:569–582.
Sachdev RNS, Ebner FF, Wilson CJ. 2004. Effect of subthreshold up and down states on the whisker-evoked response in somatosensory cortex. J Neurophysiol 92:3511–3521.
Sanchez-Vives MV, McCormick DA. 2000. Cellular and network mechanisms of rhythmic recurrent activity in neocortex. Nat Neurosci 3:1027–1034.
Schimicek P, Zietlhofer J, Anderer P, Saletu B. 1994. Automatic sleep-spindle detection procedure: aspects of reliability and validity. Clin Electroencephalogr 25:26–29.
Speckmann EJ, Elger CE. 2005. Introduction to the neurophysiological basis of the EEG and DC potentials. In: Niedermeyer E, Lopes da Silva FH, editors. Electroencephalography: basic principles, clinical applications and related fields. Philadelphia, PA: Lippincott Williams & Wilkins. p 17–29.
Steriade M, Amzica F, Contreras D. 1996. Synchronization of fast (30–40 Hz) spontaneous cortical rhythms during brain activation. J Neurosci 16:392–417.
Steriade M, Contreras D, Amzica F, Timofeev I. 1996. Synchronization of fast (30–40 Hz) spontaneous oscillations in intrathalamic and thalamocortical networks. J Neurosci 16:2788–2808.
Steriade M, Dossi RC, Nuñez A. 1991a. Network modulation of a slow intrinsic oscillation of cat thalamocortical neurons implicated in sleep delta waves: cortical potentiation and brainstem cholinergic suppression. J Neurosci 11:3200–3217.
Steriade M, Dossi RC, Pare D, Oakson G. 1991b. Fast oscillations (20–40 Hz) in thalamocortical systems and their potentiation by mesopontine cholinergic nuclei in the cat. Proc Natl Acad Sci USA 88:4396–4400.
Steriade M, McCormick DA, Sejnowski T. 1993. Thalamocortical oscillations in the sleeping and aroused brain. Science 262:679–685.
Steriade M, Nuñez A, Amzica F. 1993a. Intracellular analysis of relations between the slow (<1 Hz) neocortical oscillations and other sleep rhythms of electroencephalogram. J Neurosci 13:3266–3283.
Steriade M, Nunez A, Amzica F. 1993b. A novel slow (<1 Hz) oscillation of neocortical neurons in vivo: depolarizing and hyperpolarizing components. J Neurosci 13:3252–3265.
Steriade M, Timofeev I. 2003. Neuronal plasticity in thalamocortical networks during sleep and waking oscillations. Neuron 37:563–576.
Steriade M, Timofeev I, Grenier F. 2001. Natural waking and sleep states: a view from inside neocortical neurons. J Neurophysiol 85:1969–1985.
Stern EA, Jaeger D, Wilson CJ. 1998. Membrane potential synchrony of simultaneously recorded striatal spiny neurons in vivo. Nature 394:475–478.
Stern EA, Kincaid AE, Wilson CJ. 1997. Spontaneous subthreshold membrane potential fluctuations and action potential variability of rat corticostriatal and striatal neurons in vivo. J Neurophysiol 77:1697–1715.
Timofeev I, Contreras D, Steriade M. 1996. Synaptic responsiveness of cortical and thalamic neurones during various phases of slow sleep oscillation in cat. J Physiol 494:265–278.
Timofeev I, Grenier F, Bazhenov M, Sejnowski TJ, Steriade M. 2000. Origin of slow cortical oscillations in deafferented cortical slabs. Cereb Cortex 10:1185–1199.
Timofeev I, Grenier F, Steriade M. 2001. Disfacilitation and active inhibition in the neocortex during the natural sleep-wake cycle: an intracellular study. Proc Natl Acad Sci USA 98:1924–1929.
Vanhatalo S, Palva JM, Holmes MD, Miller JW, Voipio J, Kaila K. 2004. Infraslow oscillations modulate excitability and interictal epileptic activity in the human cortex during sleep. Proc Natl Acad Sci USA 101:5053–5057.
Vanhatalo S, Voipio J, Kaila K. 2005. Full-band EEG (FbEEG): an emerging standard in electroencephalography. Clin Neurophysiol 116(1):1–8.
Volgushev M, Mukovski M, Chauvette S, Boucetta S, Timofeev I. 2004. The onsets of active states in the neocortical neurons: how synchronous are they? Society for Neuroscience Abstracts Program No. 638.2.
Volgushev M, Pernberg J, Eysel UT. 2003. Gamma-frequency fluctuations of the membrane potential and response selectivity in visual cortical neurons. Eur J Neurosci 17:1768–1776.